The Seasonal Upwelling in the Gulf of Guinea Due to Remote Forcing[1]

DAVID ADAMEC AND JAMES J. O'BRIEN

Departments of Meteorology and Oceanography, Florida State University, Tallahassee 32306

ABSTRACT

A linear model on an equatorial β plane is integrated over a 120-day period in a basin that approximates the tropical Atlantic Ocean. An increase in the westward wind stress of 0.025 N m^{-2} in the western Atlantic excites an equatorially trapped Kelvin wave that propagates eastward along the equator, moves poleward at the eastern boundary, and produces upwelling throughout the Gulf of Guinea. Cases that study the effects of nonlinearities and the inclusion of a northward wind stress are included. Nonlinearities are shown to have the effect of amplifying the effects of the Kelvin wave and prolonging the upwelling event. The inclusion of a southerly wind stress in the eastern basin provides a secondary mechanism for upwelling south of the equator along the eastern basin. Local winds cannot account for the seasonal upwelling in the Gulf of Guinea. The simple baroclinic ocean model is integrated from rest. The effects of mean currents and bottom topography are not considered in detail.

1. Introduction

Coastal upwelling is a dramatic event during which warm nearshore water is replaced from below by cold nutrient-rich water. The most prominent upwelling areas are located at the western coasts of continents where an equatorward wind, due to the subtropical high, forces an offshore Ekman drift of the surface water.

Along the equator, upwelling is also an important event. The dynamics of equatorial upwelling must be different from those of coastal upwelling since equatorial upwelling is an oceanic event. Observations of upwelling at several locations along the equator raise questions as to whether the upwelling is an event characteristic along the entire equator or whether, in certain areas along the equator, upwelling is produced and subsequently transmitted to other areas.

Another important upwelling area is located along the northern boundary of the Gulf of Guinea (Fig. 1). Every summer for a period from early July through September upwelling is an important feature along the Gulf of Guinea coast. Several attempts to model the upwelling event have met with little success. Both the local winds and the local ocean circulation appear to be inadequate explanations for the upwelling (Houghton, 1976).

The summer meteorology of the equatorial Atlantic basin is dominated by westward trades in the west and northward monsoonal flow in the east.

The subtropical anticyclones over the ocean are most intense during the summer with an average daily surface pressure over 1025 mb (Atkinson, 1971). The trades in the west are broader in the summer than in the winter. The general pattern for the tropics is a continuous belt of high pressure interrupted only by the heat lows located over the continents. This pattern sets up a pressure gradient from land to sea.

During GATE (summer 1974), a Soviet ship, the R.V. *Passat*, located on the equator at 10°W, recorded a drop in the sea surface temperature prior to the onset of the seasonal upwelling in the Gulf of Guinea (Moore *et al.*, 1978). The time delay between the upwelling event observed by the *Passat* and the Gulf of Guinea upwelling suggest the phase speed of a first baroclinic mode Kelvin wave. A Kelvin wave propagating along the equator would be a remote driving mechanism for the upwelling and would be evidence for the equator as a waveguide. A more detailed presentation of the observational evidence for the equator as a waveguide can be found in Moore *et al.* (1978). O'Brien *et al.* (1978) presented a discussion of the dynamics related to this hypothesis. This paper is an expansion of that short paper with additional results.

In 1974 a concentrated effort at measuring the summer upwelling in the Gulf of Guinea was made by the Ghana Fishery Research Unit. The northern coast of the Gulf of Guinea is, for the most part, zonally oriented along 5° north, but there are limited areas along the coast where the local winds are favorably oriented for forcing wind-driven upwelling. At Tema, Ghana, the wind is from the

[1] Contribution 139 of the Geophysical Fluid Dynamics Institute, Florida State University.

southwest, nearly parallel to the coast with a slight onshore component. For times immediately preceding and at the beginning of the upwelling period, there is no significant change in the local wind structure (Houghton, 1976). There is poor correlation between local winds and the upwelling event. Local winds, therefore, seem to be insufficient to drive the upwelling. It is possible near capes, such as at Tema, that the seasonal upwelling is enhanced by local winds (Bakun, 1978). Thus, a possible explanation for the Gulf of Guinea upwelling is that upwelling occurs at specific locations along the Gulf of Guinea and that local ocean circulations advect the colder water to other regions. Observations show that the local surface flow is dominated by the eastward Guinea Current, accompanied by a westward undercurrent. During the initial stages of upwelling, the nearshore temperatures drop rapidly. Houghton (1976) finds no time delay in the drop in temperatures along the coastal areas near Tema to suggest advection. The Gulf of Guinea upwelling is a large-scale event characteristic of an entire region and lasts for several months. The only significant variations in the ocean flow occur as part of the upwelling event. It seems unlikely that the local circulation is responsible for the upwelling.

Since there is no correlation between local winds and nearshore temperatures or changes in the local ocean circulation, it becomes necessary to look elsewhere for a forcing mechanism. The *Passat* observation suggest a forcing that is oceanic in origin. Previous investigations by Moore (1968) and Moore and Philander (1977) discuss the upwelling due to a Kelvin wave excited by an increase in the zonal wind stress in an unbounded ocean. In the tropical Atlantic significant increases in the zonal wind stress occur 3000 km from the Gulf of Guinea coast.
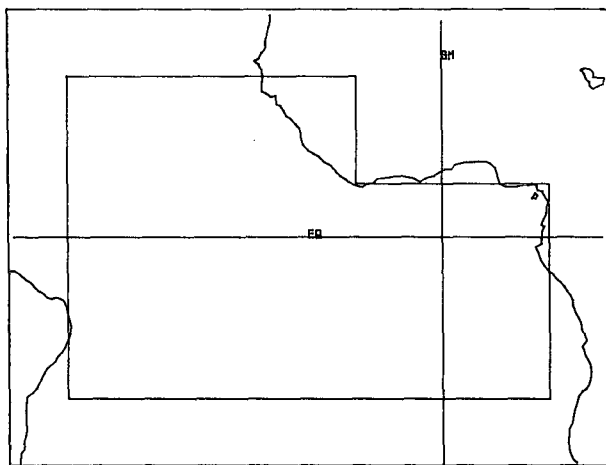

Fig. 1. Comparison of model geometry with the equatorial Atlantic basin. The model extends 5000 km zonally and 3000 km meridionally.
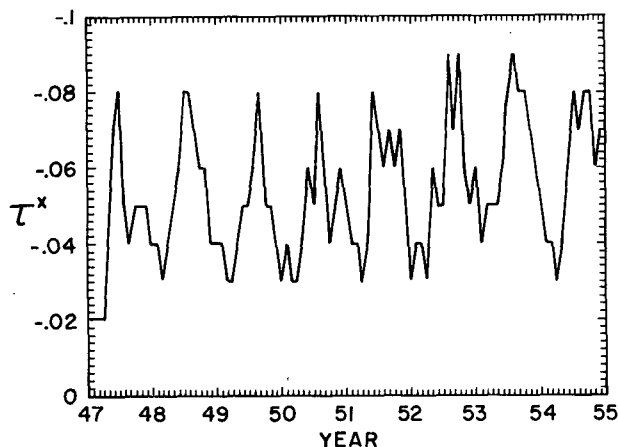

Fig. 2. Monthly wind stress averages (Bunker, 1976) for Marsden square 303 (30–40°W, 0–10°S) for the years 1947–54.

Katz (1977) finds that during the summer of 1974 there was an increase in the oceanic zonal pressure gradient in the western equatorial Atlantic. In order to determine whether this was part of an annual cycle, Katz reviewed the synoptic observations of the *Equalent* I and II experiments (1963) and reports from the R.V. *Crawford* during the International Geophysical Year (1958). The *Equalent* I experiment shows the almost complete disappearance of an oceanic zonal pressure gradient in March, while both the GATE and *Equalent* experiments show maximum values in the month of August, with high values maintained up to November. The pattern of low values in late winter and high values in late summer occurs throughout a band 5° north and south of the equator in the western Atlantic.

The correlation between the ocean zonal pressure gradient and the zonal wind stress is high. There are four supporting observations that show the wind stress has minimal values when the zonal pressure gradient is almost zero. Fig. 2 shows clearly the annual cycle of the zonal wind stress. Maximum values are attained in midsummer and minimum values in early spring. The occurrence of the oceanic zonal pressure gradient in the western Atlantic during the period of increased westward trades is consistent with the occurrence of low-frequency Kelvin waves.

It is the purpose of this paper to show that an increase in the westward trades in the western Atlantic excites an equatorially trapped Kelvin wave which propagates eastward along the equator. The Kelvin wave then propagates poleward as a coastal Kelvin wave and produces the upwelling event along the Gulf of Guinea coast. The review by Moore and Philander (1977) contains excellent background information on the dynamics of equatorial waves. The basic model is a simple, linear, hydrostatic and baroclinic ocean. The effects of nonlinearities and mean currents are considered.

2. The model

The irregular geometry of the equatorial Atlantic basin (Fig. 1) distinguishes the upwelling problem in the Gulf of Guinea from prior analytical work. The approximated basin extends 5000 km zonally and 1500 km either side of the equator. The east-west boundary representing the northern boundary of the Gulf of Guinea extends 2000 km westward of the eastern boundary, and is located 500 km north of the equator.

The governing equations for a two-layer, linear inviscid flow with a flat bottom are

$$u_{1t} - \beta y v_1 + P_{1x} = \tau^x/\rho_1 H_1, \qquad (1a)$$

$$v_{1t} + \beta y u_1 + P_{1y} = \tau^y/\rho_1 H_1, \qquad (1b)$$

$$h_{1t} + H_1(u_{1x} + v_{1y}) = 0, \qquad (1c)$$

for the upper layer, and

$$u_{2t} - \beta y v_2 + P_{2x} = 0, \qquad (2a)$$

$$v_{2t} + \beta y u_2 + P_{2y} = 0, \qquad (2b)$$

$$h_{2t} + H_2(u_{2x} + v_{2y}) = 0, \qquad (2c)$$

for the lower layer. A list of variables appears at the end of the text. Most of the symbols have their common usage in oceanography.

If the fluid is hydrostatic and the lower layer is assumed to adjust so that $\nabla P_2 = 0$, then the system of equations reduces to

$$u_t - \beta y v + g'h_x = \tau^x/\rho H, \qquad (3a)$$

$$v_t + \beta y u + g'h_y = \tau^y/\rho H, \qquad (3b)$$

$$h_t + H(u_x + v_y) = 0, \qquad (3c)$$

where $g' = g(\rho_2 - \rho_1)/\rho_2$.

The free modal response to Eqs. (3) includes the effects of inertia-gravity, Rossby and mixed Rossby-gravity waves. Another interesting free response to Eqs. (3) is the flow on a β plane when values of the meridional velocity are made equal to zero. With values of $v = 0$, cross differentiation of Eqs. (3a) and (3c) yields the wave equation

$$u_{tt} - (g'H)u_{xx} = 0, \qquad (4)$$

which has a solution

$$u(x,y,t) = G(y)F(x \pm ct), \qquad (5)$$

where $c = (g'H)^{1/2}$ and F is any function of $x \pm ct$; F need not be sinusoidal or periodic.

It is possible to solve for G by eliminating in favor of u between Eqs. (3b) and (3c) to obtain

$$-\beta y u_t + g'H u_{xy} = 0. \qquad (6)$$

A substitution of (5) into (6) yields

$$-\beta y(\pm c[F]G) + g'H[F][G] = 0, \qquad (7)$$

where square brackets denote differentiation.

The solution of (7) is

$$G(y) = a \exp[\pm\tfrac{1}{2}(y/L_e)^2]. \qquad (8)$$

Since any physical solution must be bounded away from the equator, only the minus sign is permissible so one may write

$$u(x,y,t) = aF(x - ct) \exp \text{ form}, \qquad (9)$$

where $L_e = (c/\beta)^{1/2}$ is the internal equatorial radius of deformation. A typical value of L_e for the equatorial Atlantic is $\sim$225 km. The result is an eastward propagating Kelvin wave, with phase speed c, which is equatorially trapped with an e-folding distance of $\sqrt{2}\,L_e = 350$ km.

Along a boundary away from the equator, the e-folding length is the internal Rossby radius of deformation, $L_c = c/\beta y$. As the Kelvin wave moves toward increasing y, the Rossby radius of deformation decreases. Conservation of energy requires that, as the trapping scale of the wave is reduced, the amplitude of the response away from the equator increases. A typical value of L_c along the Gulf of Guinea coast is 100–200 km. Therefore, any impulse of equatorial origin will increase in amplitude but the speed of propagation will remain unchanged.

The addition of viscous effects to Eqs. (3) yields

$$u_t - \beta y v + g'h_x - A\nabla^2 u = \tau^x/\rho H, \qquad (10a)$$

$$v_t + \beta y u + g'h_y - A\nabla^2 v = \tau^x/\rho H, \qquad (10b)$$

$$h_t + H(u_x + v_y) = 0. \qquad (10c)$$

The system of Eqs. (10) is the simplest formulation of the first baroclinic modal response, and is sometimes referred to as the reduced gravity formulation. In a remarkable paper on the Somali current dynamics, Lin and Hurlburt (1978) use an identical formulation to effectively simulate many of the features of the Somali current.

3. Results

Using Eqs. (10), a numerical simulation of the oceanic response to an increase of the wind stress was performed. All calculations were made on an equatorial β plane, with grid resolution of 25 km in both the x and y directions. The undisturbed depth of the upper layer is taken to be 50 m, with a density difference of 2.0 kg m^{-3} between layers. The time step is $\frac{1}{8}$ day. All calculations are performed on a flat-bottomed ocean. A simple Laplacian representation of viscous effects with a horizontal eddy viscosity of 10^2 m^2 s^{-1} is used to bring the flow to zero at the boundaries.

Three major cases are studied: a standard linear case that looks at the oceanic response to the increase of 0.025 N m^{-2} in the westward wind stress over the western 1500 km of the basin (Fig. 3); a

nonlinear case similar to the standard linear case but including advective effects, local depth in the stress term and nonlinearities in the continuity equation with a reduction from 0.025 N m^{-2} in the increase of the westward wind stress; and a third case which is similar to the first but includes an increase of 0.025 N m^{-2} in the meridional stress over the eastern 1800 km of the basin. The wind stress value agrees with Fig. 2. Other cases varying the magnitude and location of the wind stress and moving the boundaries were also run. In all cases the wind is impulsively started at day 0, and kept constant throughout a 120-day integration. A typical profile of the wind stress is shown in Fig. 3. The specific goal was to look at oceanic changes in response to a change in the wind. No mean flow is included. The actual circulation would be the superposition of the response cases with the mean flow, except for the nonlinear case.

A staggered grid in space was used to increase resolution with a minimal amount of core storage. The grid structure defines normal velocity components on the boundary and the reflection of the tangential velocity as a computational point outside the boundary. A typical stencil for interior points is shown in Fig. 4. The equations are finite differenced, using leapfrog for the time derivatives and lagged-in-time for the diffusive terms.

At this point it is convenient to adopt a convention when discussing the solutions near boundaries. There are two separate eastern and northern boundaries. The eastern boundary extending 1500 km south of the equator to 500 km north will be referred to as the south-eastern (S-E) boundary. The eastern boundary extending 500 km north of the equator to 1500 km north will be referred to as the
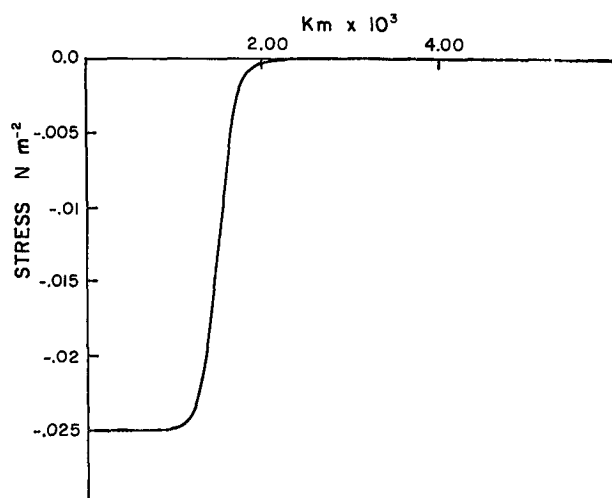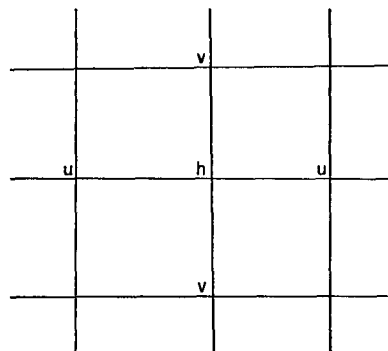

FIG. 4. Stencil of the staggered grid in space used for the computations. Normal velocities are defined on the boundaries.

north-eastern (N-E) boundary. The northern boundary extending from 3000 to 5000 km east of the western boundary is designated the south-northern (S-N) boundary, and the northern boundary extending 3000 km from the western boundary is designated the north-northern (N-N) boundary.

a. Standard linear case

A simple view of the oceanic response near the equator to a westward wind stress is the replacement of surface water with subsurface water due to Ekman divergence near the equator. The vertical motion of the subsurface water is traceable by the movement of the density interface. An upward movement of the interface produces a negative height anomaly, indicating upwelling. Fig. 5 shows a well-defined elliptically shaped upwelling region centered on the equator in the western basin. The upwelling is symmetric about the equator due to symmetric forcing in the western basin and has a maximum value of 12 m. The latitudinal extent of the upwelling response is 700 km, which is in agreement with the internal equatorial radius of deformation.

There is a corresponding minimum u component of -0.41 m s^{-1} that accompanies the upwelling at day 10. Fig. 6 shows that initially there is a linear increase of the westward current in low latitudes, which gives rise to a Yoshida jet (Yoshida, 1959). The minimum values of u are located at the equator. This is consistent with Eq. (9), which states that values of the u component must decay exponentially away from the equator. The oscillations observable in Fig. 6 are a result of the inertia-gravity waves excited by the impulsive start of the wind stress.

Another important result of Eq. (9) is that the Kelvin wave excited by the wind stress must propagate to the east. Fig. 7 clearly shows this result. The maximum upwelling is now 800 km from the

FIG. 3. The x dependence of a wind stress extending 1500 km zonally. The value 1500 km is chosen because it is at that point the value of the wind stress is half the maximum value.
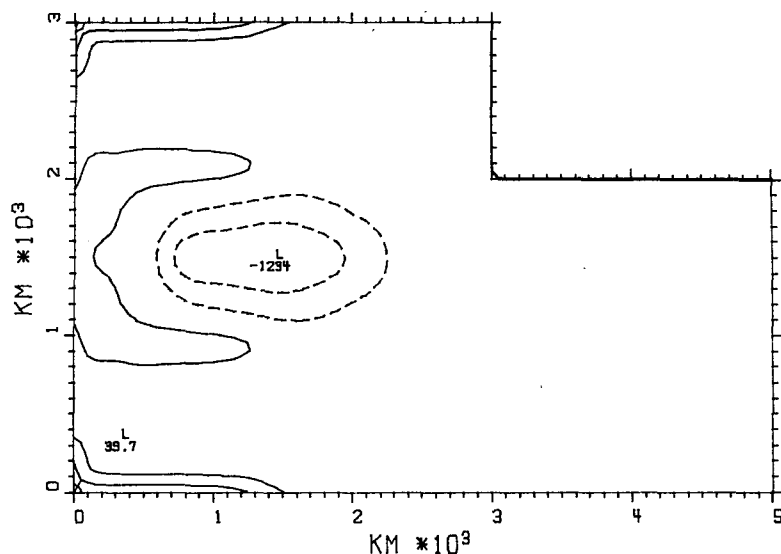
FIG. 5. Height field anomaly contours for the standard linear case at day 10. The contour interval is 5.0 m with negative values dashed.

S-E boundary and has increased to a value over 25 m. The leading edge of the Kelvin wave is producing upwelling along the S-N boundary. The eastern propagation of the Kelvin wave is more clearly shown in O'Brien et al. (1978). Note that in the western basin the flow is adjusting so that the pressure gradient balances the wind stress. This is consistent with the observations of Katz (1977).

Since the linear Kelvin wave is nondispersive, it retains its shape as it propagates. The local minimums in the upwelling that are evident in the west-

ward current are caused by the Rossby wave reflection of a portion of the Kelvin wave energy from the N-E boundary. McCreary (1976) and Moore (1968) discuss the dynamics in detail. The Kelvin wave cannot be part of the reflected solution at an eastern boundary, since it may only propagate its energy eastward along the equator [as derived in Eq. (9)]. Equatorial Rossby waves propagate their energy westward with a phase velocity one-third that of the Kelvin wave. Although eastward propagating Rossby waves are an admissible solution, they can-
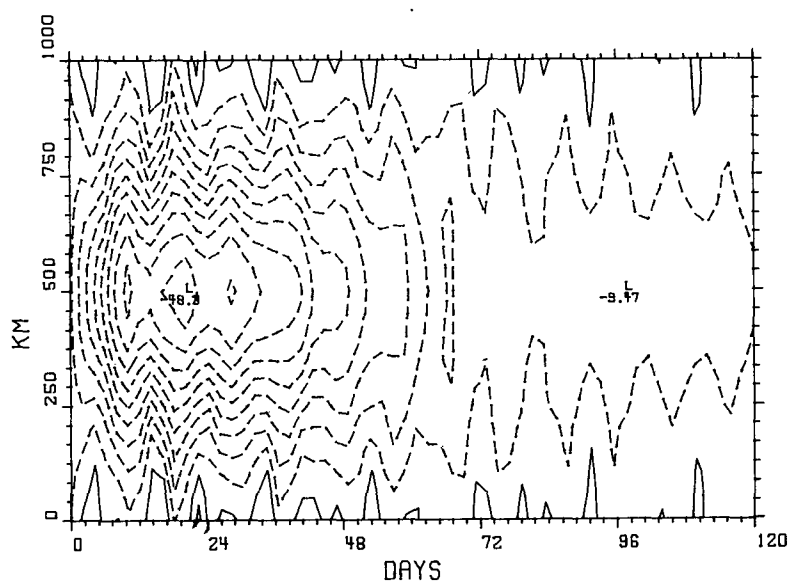

FIG. 6. Time-dependent contours of the u component of the flow for a section 1000 km from the western boundary running 500 km either side of the equator. The contour interval is 0.05 m s^{-1}.
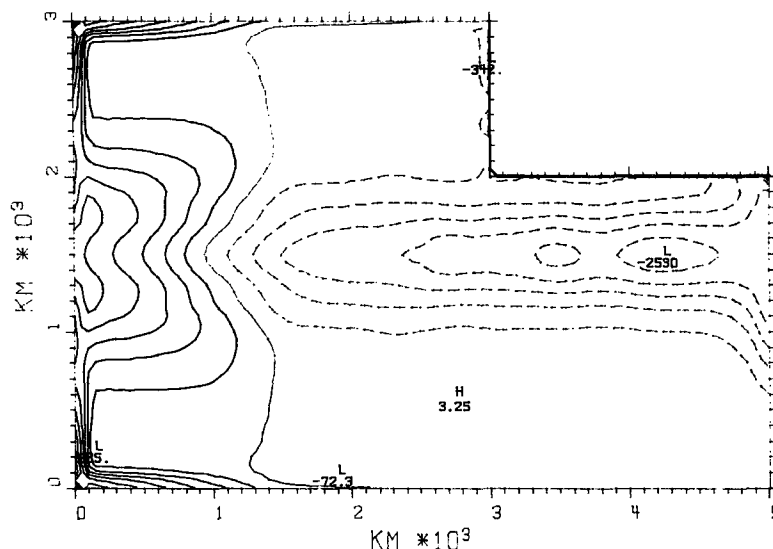
FIG. 7. Height field anomaly contours for the standard linear case at day 50.
The contour interval is 5.0 m.

not account for the strong upwelling along the Gulf of Guinea.

It has been stated earlier in this paper that the mean flow is not included in this formulation of the problem. Philander (1978a) investigates the influence of an equatorial undercurrent on the propagation of equatorial waves. He finds that the Kelvin wave will propagate free from the effects of the undercurrent if the propagation speed of the Kelvin wave is large compared with the speed of the undercurrent (0.75 m s^{-1}), and if the latitudinal extent of the Kelvin wave is larger than the extent of areas

where the undercurrent has high speeds (200 km). As a result, superposition is possible and no critical layers develop that disallow the existence of a Kelvin wave.

The flow produced by the Kelvin wave along the S-N boundary is opposite in direction to phase propagation. The eastward propagating Kelvin wave produces a flow to the west. The westward propagating wave along the S-N boundary produces a flow to the east. Both of these results are clearly seen in the velocity vectors at day 60 shown in Fig. 8. The coastal Kelvin wave is producing an east-
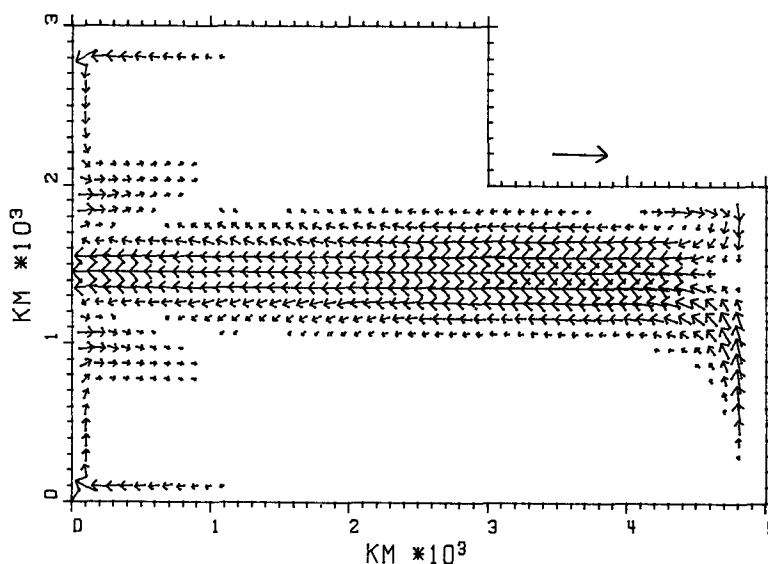
FIG. 8. Velocity vectors for the standard linear case at day 60. The length of the arrow is proportional to the magnitude of the flow. No value below 0.05 m s^{-1} is plotted.
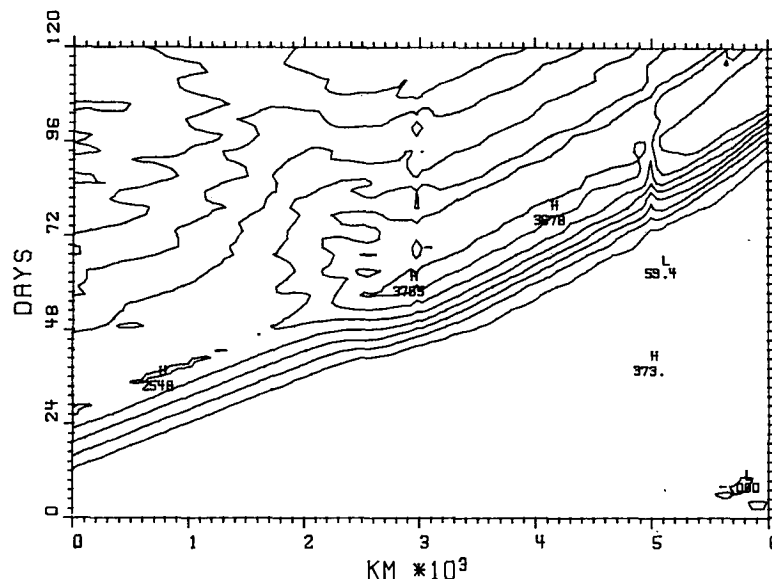
FIG. 9. Time-dependent contours of the height field anomaly for a section running along the equator and boundaries. The section 0–2500 km is the eastern 2500 km of the equator, 2500–3000 km is the south-eastern boundary north of the equator, 3000–5000 km is the south-northern boundary, and 5000–6000 km is the north-eastern boundary. The contour interval is 5.0 m (from O'Brien et al., 1978).

ward flow along the eastern section of the S-N boundary. Further west, the flow is to the west in response to the trailing edge of the eastward propagating wave at the equator. Along the S-N boundary, u changes sign from negative to positive going east. This produces a positive contribution to divergence, u_x. Continuity requires that this be an area of upwelling. The westward propagating Kelvin wave along the S-N boundary contributes constructively to the eastward Guinea Current. This is consistent with observations which show an increase in the eastward flow during upwelling (Picaut and Verstraete, personal communication).

As the Kelvin wave propagates along the boundaries, the amplitude of the response increases with increasing y (Fig. 9). The straight parallel contours in the lower part of Fig. 9 show the Kelvin wave impulse propagating along the equator and then along the coast. The slope of the lines is the reciprocal of the phase speed of the Kelvin wave. Along the S-N boundary, the maximum upwelling values are near 38 m, while at the equator the maximum value is 25 m. This result is expected. The Rossby radius of deformation at 500 km N is 100 km, in

contrast to the 225 km equatorial radius of deformation. The Kelvin wave energy is now trapped on a smaller scale, and, as a result, the wave impulse amplifies.

It is possible to determine the length of the upwelling period at the S-N boundary by following the change in the height field anomaly at 4000 km in Fig. 9. This point is 1000 km west of the S-E boundary. If a height change of −20 m is used as a reference to determine whether or not there is significant upwelling, then there are 45 days of significant upwelling at this point. Observations along the Gulf of Guinea show that the upwelling is on the order of three months. Effects of nonlinearities will slow the phase propagation of the Kelvin wave and, consequently, prolong the upwelling event. In other words, nonlinear effects are required if the observed seasonal span of the upwelling event is to be predicted.

b. Nonlinear case

The inclusion of nonlinear terms has two effects on the Kelvin wave: 1) a reduction of the phase speed and 2) an amplification of the wave's effects. The governing equations for the system become

$$
\left.
\begin{aligned}
u_t + uu_x + vu_y - \beta yv + g'hx - A\nabla^2 u &= \tau^x/\rho(H + h) \\
v_t + uv_x + vv_y + \beta yu + g'hy - A\nabla^2 v &= \tau^y/\rho(H + h) \\
h_t + [(H + h)u]_x + [(H + h)v]_y &= 0
\end{aligned}
\right\} .
\tag{11}
$$

Nonlinearities in the continuity equation make the phase speed of the Kelvin wave $[g'(H + h)]^{1/2}$, as compared with $[g'H]^{1/2}$ for the linear case. In an upwelling region h is negative. Therefore, the phase speed for the nonlinear case is less than the phase speed for the linear case in an upwelling region. A second mechanism for slowing the Kelvin wave is the Doppler shift which occurs as a result of advective effects. Since the flow associated with the Kelvin wave is opposite in direction to the phase propagation, the Kelvin wave moves at a slower rate.

The amplification of the wave's effects occurs because of nonlinearities in the stress term. The inclusion of local depth in the stress term $(\tau/\rho)(H + h)$ causes the denominator to become smaller in magnitude in a forced region. This effect is coupled with the reduced phase speed of the Kelvin wave. The Kelvin wave is present in the forced region for a longer period of time. The effect of the longer time-scale forcing, coupled with a higher effective stress, leads to an amplification of the wave. A value of 0.0125 N m^{-2} is used for the wind stress in this study to prevent upwelling greater than 50 m and to keep the effective stress $\tau^x/\rho(H + h)$ bounded.

The nonlinear Kelvin wave is dispersive. Maximum values of upwelling occur on the equator; consequently, the slowest phase speeds occur there. The effect of having a faster phase propagation away from maximum upwelling values is to elongate the leading edge of the Kelvin wave and flatten the trailing edge (Fig. 10). The maximum upwelling is at the center of the basin, as compared to the standard linear case in which it was 1700 km more to the east at this point in the integration. However, the position of the leading edge of the Kelvin wave is only slightly different from the linear case. Both the leading and trailing edges of the Kelvin wave propagate with a phase speed close to that of the linear wave, since the magnitude of h is small.
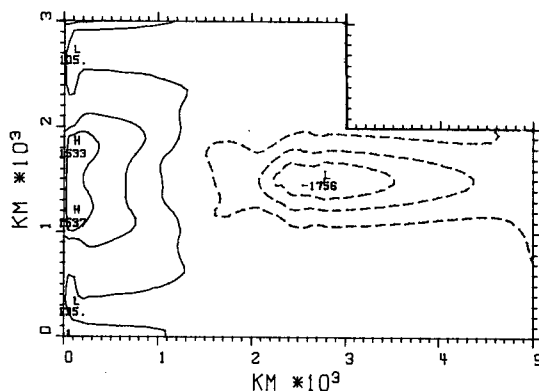
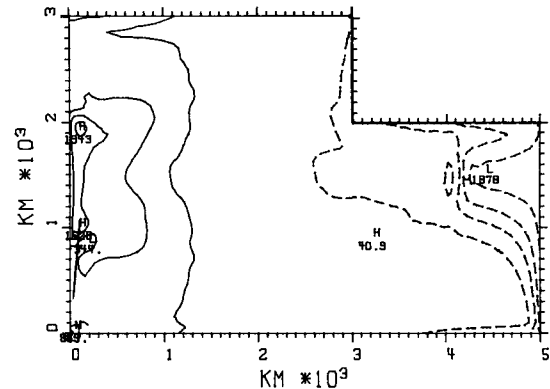Eventually the faster propagating trailing edge of

FIG. 11. As in Fig. 10 except at day 80.

the Kelvin wave overtakes the maximum upwelling values. This creates an instability in the wave, causing it to break. Fig. 11 shows that the wave has broken before the maximum upwelling could reach the S-E boundary. the result is a mesoscale eddy behind the still flattened trailing edge of the wave. The upwelling maximum is now close to 19 m. The effect of coastal amplification is not evident yet.

The nonlinear solution does not exhibit amplification of the wave impulse as in the linear case. This result is consistent with the works of Hurlburt and Thompson (1976) and Hurlbert et al. (1976).

Numerical solutions reveal that upwelling is still a feature along the S-N boundary at day 110. Although the values are smaller in the nonlinear case than in the linear case, the upwelling is still significant. The lower magnitude of the wind stress is responsible for the lower values of upwelling. The full 0.025 N m^{-2} stress could not be used, since it produced over 50 m of upwelling in the forced region before day 30. The result is an effective stress too large for this particular model to handle. The salient results of adding nonlinearities to the problem are the amplification of the upwelling event and the creation of a mechanism for slowing the phase speed, which produces an upwelling event on the same time scale as the observed event.

c. South and east wind case

Coastal upwelling along the west coast of Africa south of the equator is a well-documented event. The southerly winds over the eastern Atlantic are favorably oriented for wind-induced upwelling along Africa south of the equator but not north of the equator. An increase of 0.025 N m^{-2} in the northward wind stress over the eastern 1800 km of the basin is incorporated into the standard linear case. The x dependence of the stress is much the same as shown in Fig. 3. The increase of wind stress in the western basin remains unchanged. The addition of a northward wind stress in the model forces an Ekman

FIG. 10. Height field anomaly contours for the nonlinear case at day 50. The contour interval is 5.0 m.
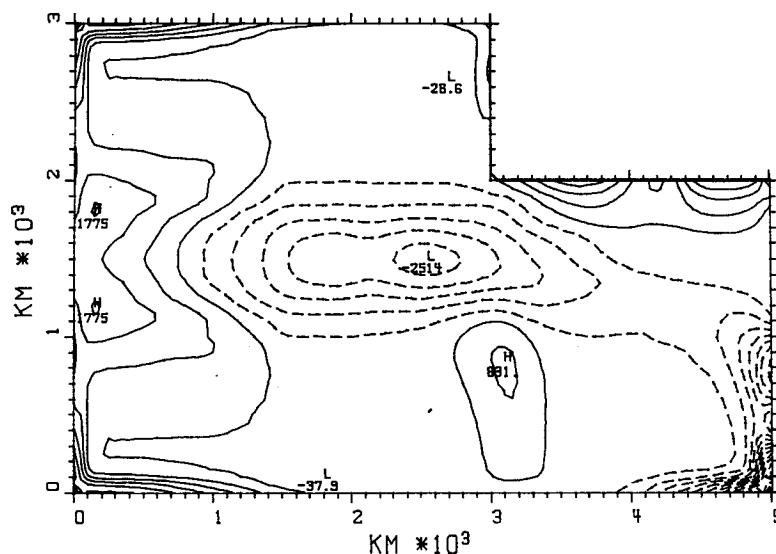
FIG. 12. Height field anomaly contours for the south and east wind case
at day 30. The contour interval is 5.0 m.

divergence south of the equator and an Ekman convergence north of the equator. The result is upwelling south of the equator and downwelling north of the equator along the S-E boundary, as shown in Fig. 12. Both the upwelling and downwelling exhibit a double pulse effect. This solution is consistent with the eastern equatorial solution of the Hurlburt and Thompson (1976) model of the Somali current. The flow near the neastern boundary is strongly coupled with the inertial oscillations, exciting a train of coastally trapped, poleward propagating Kelvin waves. The period of the oscillation is 16.2 days. The Kelvin waves propagate with a phase speed of 86 km day^{-1}. The result is a 1400 km separa-

tion between the leading edge of the pulses on both sides of the equator.

Solutions for later times reveal that the inertial oscillations are damped. Near the western extreme of the southerly winds, non-symmetric forcing excites a mixed Rossby-gravity wave. The mixed Rossby-gravity wave propagates eastward and, upon reaching the S-E boundary, damps the inertial oscillations. As a result, there is no mechanism to excite subsequent coastal Kelvin waves. Fig. 13 shows that along the S-N boundary the production of the downwelling pulses has been damped, and upwelling is now taking place along the boundary in response to the Kelvin wave excited in the western
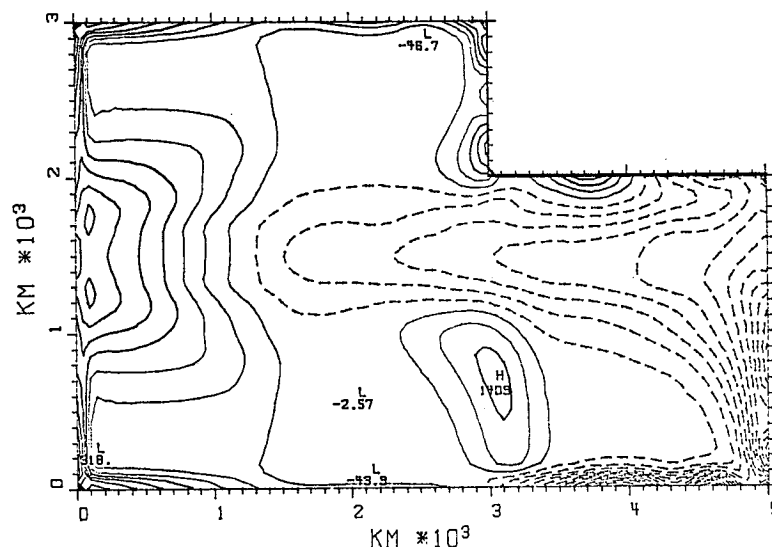

FIG. 13. As in Fig. 12 except at day 60.

basin. At no point in the integration was upwelling forced by the meridional wind along the S-N boundary. Upwelling is present, however, along the S-E boundary south of the equator during the entire integration. This case demonstrates that the large-scale northward local winds over the Gulf of Guinea cannot account for the seasonal upwelling event.

d. Results of other cases

Additional case studies investigated the linear response of a basin with the S-N moved to 1000 and 1500 km north of the equator. The results revealed no change in the Kelvin wave excited in the western basin. The phase propagation was unchanged, with the exception of the absence of Rossby wave reflection at the N-E boundary. The most significant change occurring was in the amount of upwelling along the S-N boundary. This increase in upwelling is a result of the y^{-1} dependence of the Rossby radius of deformation.

The oceanic response to varying wind stresses was also studied. There is a strong dependence of the magnitude of upwelling on the area over which the wind stress was applied. By applying the wind stress over the western 2500 km of the basin, the upwelling along the S-N boundary is increased significantly. Further studies with more realistic wind stress patterns could be used to fine-tune the model to the observed event. A time-dependent spinup of the westward wind stress was performed, with the result of a slightly longer upwelling event and a decrease in the amplitude of the response.

Philander (1978b) discusses the possibility of local forcing by the meridional wind stress for upwelling in the Gulf of Guinea. He proposes that a cross equatorial wind will produce an eastward current that is in geostrophic balance north of 2°N and a westward current south of 2°N. As a result, the isopycnals slope upward north of 2°N and produce low nearshore temperatures along the Gulf of Guinea.

4. Summary and conclusions

In this paper an attempt was made to explain the physical events linked with the seasonal upwelling in the Gulf of Guinea. Previous work by Houghton (1976) showed that neither the local winds nor the ocean circulation provide an adequate forcing mechanism. Observations during GATE suggest that the forcing may have been oceanic in origin in the form of a first baroclinic mode Kelvin wave (Moore et al., 1978). The summer increase in zonal wind stress in the western basin of the Atlantic is proposed as the forcing mechanism which excites an eastward propagating Kelvin wave, which pro-

duces upwelling as it propagates along the coastal boundaries.

The nonrectangular geometry of the equatorial Atlantic has been a major obstacle in obtaining an analytical solution of the linear problem. A numerical scheme was devised to demonstrate the first baroclinic modal response of an ocean to a changing wind system. Computations were performed using the β-plane approximation in an ocean initially at rest. The system was driven by a 0.025 N m^{-2} wind stress over the western 1500 km of the western basin.

In order to elucidate the dynamics of the upwelling, case studies with added nonlinear terms and local forcing were included to demonstrate a mechanism for lengthening the time period of the upwelling. The results of the studies warrant the following conclusions:

1) The increase of wind stress in the western basin is a remote forcing mechanism capable of producing upwelling in the Gulf of Guinea. The standard linear case produces 25 m of upwelling along the equator, and over 50 m at 500 km N. The eastward propagation of the Kelvin wave at the equator and the amplification of its effects with increasing latitude are consistent with analytic work. The u component of the flow which accompanies the Kelvin wave reaches a maximum magnitude of 0.5 m s^{-1} and is in the opposite direction to the phase propagation of the Kelvin wave. A study of the time scale of the model upwelling produced by the Kelvin wave reveals that the time period of upwelling is much shorter than the observed period. Thus, nonlinear terms must be included in this formulation.

2) Symmetric forcing in the western basin guarantees that the solution will be perfectly symmetric about the equator for early times. Any asymmetries found in the solution must be the result of the asymmetric geometry of the eastern basin. Initially the solution does exhibit the symmetry predicted by linear theory, but by day 50 asymmetries are evident. The asymmetries are due to different propagation paths of the Kelvin wave and to Rossby wave reflection at boundaries. Symmetry in the western basin is a feature throughout the entire integration.

3) The addition of nonlinear terms has the effect of broadening the time scale of the upwelling and amplifying its effects. The reduced propagation speed is due to a Doppler shift and to the inclusion of nonlinearities in the continuity equation. The amplification is a result of the inclusion of local depth in the stress term. The effect of amplification due to increasing latitude is not evident in the nonlinear case. This result is consistent with a nonlinear study by Hurlburt et al. (1976), who found that the Kelvin wave excited westward propagating Rossby waves as it propagated along an eastern boundary. At in-

creased latitudes the Rossby waves are less energetic and become less distinguishable.

4) The inclusion of local winds provides a secondary mechanism for upwelling south of the equator on an eastern boundary. This is to be expected from classical Ekman theory. At no point do local winds force upwelling north of the equator. The flow near the eastern boundary becomes coupled with the inertial oscillations and excites a train of coastal Kelvin waves. This is consistent with the work of Hurlburt and Thompson (1976) on the Somali current. The trapped inertia-gravity oscillations are damped when an eastward propagating mixed Rossby-gravity wave excited at the western limit of the northward winds reaches the eastern boundary.

Questions regarding whether or not the equatorial ocean is capable of propagating energy zonally arise when discussing modes of a solution. More specifically, is the Atlantic floor an adequate reflector for setting up a standing baroclinic mode? How do local currents affect modes in an equatorial ocean? The model used for this paper is undoubtedly too simple to answer these questions. Further studies which include topographic effects, coastline geometry and mean flow are essential to a complete understanding of these questions.

APPENDIX

List of Symbols

A	horizontal eddy viscosity
c	phase speed of a Kelvin wave
f	Coriolis parameter
g'	reduced gravity $[=g(\rho_2 - \rho_1)/\rho_2]$
h, h_1, h_2	local height field change from undisturbed depth in a layer
H, H_1, H_2	undisturbed thickness of layers
L_c	Rossby radius of deformation
L_e	internal equatorial radius of deformation
P, P_1, P_2	local pressure
t	time
u, u_1, u_2	x directed component of velocity
v, v_1, v_2	y directed component of velocity
x, y, z	tangent plane Cartesian coordinates; x positive eastward, y positive northward and z positive upward
β	df/dy
ρ, ρ_1, ρ_2	density of seawater
τ^x	x-directed tangential stress at the surface
τ^y	y-directed tangential stress at the surface

REFERENCES

Atkinson, G. D., 1971: Forecasters' guide to tropical meteorology. Air Weather Service, USAF.

Bakun, A., 1978: Guinea Current upwelling. *Nature* **271**, 147–150.

Bunker, A. F., 1976: Computations of surface energy flux and annual air-sea interaction cycles of the North Atlantic Ocean. *Mon. Wea. Rev.*, **104**, 1122–1140.

Houghton, R. W., 1976: Circulations and hydrographic structure of the Ghana continental shelf during the 1974 upwelling. *J. Phys. Oceanogr.*, **6**, 909–924.

Hurlburt, H. E., and J. D. Thompson, 1976: A numerical model of the Somali current. *J. Phys. Oceanogr.*, **6**, 646–664.

——, J. C. Kindle and J. J. O'Brien, 1976: A numerical simulation of the onset of El Niño. *J. Phys. Oceanogr.*, **6**, 621–631.

Katz, E. J., 1977: Zonal pressure gradient along the equatorial Atlantic. *J. Mar. Res.*, **35**, 293–307.

Lin, L., and H. E. Hurlburt, 1978: Maximum simplification of nonlinear Somali current dynamics. *Proceedings of IUTAM/IUGG Symp. on Monsoon Dynamics* (in press).

McCreary, J. P., 1976: Eastern tropical ocean response to changing wind systems with application to El Niño. *J. Phys. Oceanogr.*, **6**, 632–645.

Moore, D. W., 1968: Planetary-gravity waves in an equatorial ocean, Ph.D. thesis, Harvard University, 201 pp.

——, and S. G. H. Philander, 1977: Modelling of the tropical oceanic circulation. *The Sea*, Vol. 6, E. Goldberg *et al.*, Eds., Interscience-Wiley, 319–361.

——, P. Hisard, J. McCreary, J. Merle, J. J. O'Brien, J. Picaut, J-M. Verstraete and C. Wunsch, 1978: Equatorial adjustment in the eastern Atlantic. Submitted to *Geophy. Res. Lett.*

O'Brien, J. J., D. Adamec and D. W. Moore, 1978: A simple model of upwelling in the Gulf of Guinea. Submitted to *Geophy. Res. Lett.*

Philander, S. G. H., 1978a: Equatorial waves in the presence of the equatorial undercurrent. Submitted to *J. Phys.Oceanogr.*

——, 1978b: Upwelling in the Gulf of Guinea, 1978. Submitted to *J. Mar. Res.*

Yoshida, K., 1959: A theory of the Cromwell Current and of equatorial upwelling, *J. Oceanogr. Soc. Japan*, **15**, 154–170.